Application of Spectral Estimation Methods to the Design of a Multispectral 3D Camera

Réjean Baribeau†
National Research Council Canada, Ottawa, Ontario, CANADA

This article reports on the colorimetric improvement of a multispectral 3D digitizer through scanning at a small number of near-optimal wavelengths. Optimal wavelengths were first investigated theoretically based on the criterion of minimal color differences over some sets of reflectance curves using PCA-based and spline-based spectral estimation methods. Sets of three, four and five optimal sampling wavelengths were derived to within ±5 nm for each one based on the spread of variation for different combinations of the method and the data set used for the derivation. This provided a basis for the selection of HeCd, ArKr, HeNe and DPSS commercial laser lines for which the colorimetric performance was predicted. This was then tested in the laboratory, where color rendition charts were scanned with the camera at seven wavelengths, after which the charts were computer rendered on a CRT display. Both the theoretical prediction and the experimental observation indicate that four well-chosen wavelengths are adequate for proper rendition of the charts.

Journal of Imaging Science and Technology 49: 256–261 (2005)

Introduction

The recommended practices[1] for measuring the color of reflecting objects require that the complete reflectance spectra be obtained across the visible range. This is then weighted by spectral power distributions of standard illuminants and by color matching functions of standard colorimetric observers to obtain tristimulus values that correlate with the visual perception of color. Good table-top spectrophotometers typically can record a reflectance spectrum from 380 nm to 780 nm in steps of 5 nm for a total of 81 points. Spectrophotometers are good at predicting colors under various types of illuminants and for establishing colorant formulation. The spectrophotometric approach is however impractical in traditional color imaging applications, which rely instead on pixel-wise measurements of red-, green- and blue-filtered signals. The colors measured with these 2D cameras incorporate the illumination used during image acquisition. The appearance under other illuminants and the colorant composition cannot be obtained, which can be a major drawback in applications such as art conservation and internet shopping. To overcome this limitation, multispectral 2D cameras are currently being developed[2–5] which make use of a small number of filters in addition to, or in place of, the traditional RGB filters. All these filters are usually broad band, and abundant literature has been published regarding the choice of their spectral transmittance properties. The 3D laser scanner is one class of instrument that has not so far received much attention from the color imaging community. It brings the unique challenge that color accuracy must result from proper selection of a small number of extremely narrow-band scanning lasers in combination to adequate spectral estimation methods.

This article reports recent progress on the development of a 3D multispectral laser scanner making use of four lasers. These lasers were chosen following a theoretical investigation where sets of three, four, and five optimal scanning wavelengths were determined based on the minimal average color difference over various sets of reflectance curves and for different spectral estimation methods. This choice was then tested in the lab, where color rendition charts were scanned at seven wavelengths. Colors were extracted for various subsets of the seven wavelengths and the charts were computer rendered on a CRT display. Both the theoretical prediction and the experimental observation indicate that four well-chosen wavelengths are adequate for proper color rendition of the charts.

The NRC High Resolution Color Laser Scanner

This study discusses the improvement of the colorimetric performance of a multispectral 3D laser scanner developed at the National Research Council of Canada. The scanner is designed to capture the shape and color of three-dimensional objects, such as fine art paintings and archeological artifacts,[6–8] which can then be computer rendered with high realism.[9] The camera works by projecting a laser spot on the object, which is then imaged on a CCD looking at the scene from a slightly different direction from that of the incoming beam. Spatial

Original manuscript received July 12, 2004

†Corresponding Author: R. Baribeau, rejean.baribeau@nrc-cnrc.gc.ca

coordinates of surface elements are obtained by triangulation. An autosynchronized[10] scanning mechanism allows acquisition of a line profile on the object. This line is scanned across the object and a dense mesh of spatial coordinates is obtained. With this flying spot technique, only one surface element is illuminated at any given time which makes the system immune to inter-element reflection problems.

In a three laser configuration of the camera, superimposed red (633 nm), green (532 nm), and blue (442 nm) laser beams are used for the projection, and the CCD image is split into its three components with a prism. High speed peak detection electronics extract the centroid positions and the amplitudes of the three peaks. The peak positions, along with the angular scanning angles, serve to calculate the (x,y,z) spatial coordinates of the surface elements (surfels). The amplitudes of the peaks depend on the incidence and reflection angles at the surfels, and these angles can be calculated from the (x,y,z) information. The peak amplitudes are then converted into reflectance values through a calculation that compensates for the geometric effects.[11] The peak detection circuitry has provision for the simultaneous detection of up to four peaks so a fourth laser can be added to the system without affecting the data acquisition speed (typically 10^4 points per second). If more than four lasers are to be used, they must be grouped in sets of four (or less) and the object is then digitized in multiple scans.

The reflectance values obtained for the surface elements represent true intrinsic properties of the objects and are useful for monitoring the physical state of an artifact, for example before and after some restoration work. In the case where the visual rendering of the object is important, in virtual reality applications for example, it is desirable to attribute some perceptual color values to the surface elements. With red, green and blue lasers only, it is tempting to feed the measured red, green and blue reflectances directly into the input channels of the display. This is not recommended[12] and produces a poor reproduction of the colors, which are furthermore dependent of the display. Instead, the recommended practice is to convert the camera signals into a device independent color space used as an interconnection with all the possible display devices. The next sections discuss how this conversion is best performed and identifies how many and which laser lines to use for best colorimetric results.

Methods and Data

The general approach for calculating colors from laser scanner data is to first approximate the reflectance spectrum at all wavelengths between 400 and 700 nm using interpolation and extrapolation. The estimated spectra are then used to calculate CIE tristimulus values following the recommendations of the CIE. Two spectral estimation methods were considered in this study: Principal Component Analysis (PCA) and Spline interpolation. Calculations of the mean CIE color difference were performed with these two methods on six sets of spectral data. Unconstrained optimization was used to determine the best sampling wavelengths for various combinations of method, data set, and number of wavelengths. These topics are now briefly discussed, after which results and recommendations are presented.

PCA-Based Spectral Estimation

This estimation method requires some set of basis functions, called Principal Components, derived from a collection of spectra of which the curve being estimated is a plausible representative. Our calculation of the Principal Components coincides with the method recently described by Fairman and Brill.[13] Given a collection of n spectra uniformly sampled at m (= 31 in this study) wavelengths from 400 to 700 nm in steps of 10 nm, the PCA method starts by building a matrix $\mathbf{R}$ of dimension $m \times n$ where R_{ij} is the reflectance of the j^{th} sample at wavelength λ_i, minus the average reflectance $\mathbf{R}_{\text{ave}}(\lambda_i)$ for the collection at this wavelength. Each column of $\mathbf{R}$ then represents a point in m-dimensional λ space. $\mathbf{R} \times \mathbf{R}^{\mathbf{T}}$ is proportional to the covariance matrix, and its eigenvectors $\mathbf{U}_i$, sorted in descending order of associated eigenvalues, provide a suite of orthogonal directions along which the spread of the distribution of points, in m-dimensional space, is greatest. These are the Principal Components (PCs) of the collection. The spectra in the collection are then best approximated, in a global least square sense, by a linear combination of as many of the first PCs one wishes to consider, plus the average spectrum. Formally, the coefficients for this linear combination are the mathematical projection of the spectrum under consideration on each of the PCs. These cannot be calculated if the spectrum is known at just a few wavelengths. Instead, our PCA-based spectral estimation method adjusts some coefficients by forcing the estimated curve to pass through each of the sample points. For example with three sampling wavelengths (λ_1, λ_2, λ_3) the approximation reads:

$$\mathbf{R}_{\text{estimated}} = \mathbf{R}_{\text{ave}} + a_1\mathbf{U}_1 + a_2\mathbf{U}_2 + a_3\mathbf{U}_3,$$

where

$$\begin{bmatrix} a_1 \\ a_2 \\ a_3 \end{bmatrix} = \begin{bmatrix} \mathbf{U}_1(\lambda_1) & \mathbf{U}_2(\lambda_1) & \mathbf{U}_3(\lambda_1) \\ \mathbf{U}_1(\lambda_2) & \mathbf{U}_2(\lambda_2) & \mathbf{U}_3(\lambda_2) \\ \mathbf{U}_1(\lambda_3) & \mathbf{U}_2(\lambda_3) & \mathbf{U}_3(\lambda_3) \end{bmatrix}^{-1} \begin{bmatrix} \mathbf{R}(\lambda_1) - \mathbf{R}_{\text{ave}}(\lambda_1) \\ \mathbf{R}(\lambda_2) - \mathbf{R}_{\text{ave}}(\lambda_2) \\ \mathbf{R}(\lambda_3) - \mathbf{R}_{\text{ave}}(\lambda_3) \end{bmatrix},$$

which is easily generalized to more wavelengths. Occasionally an estimated spectrum has excursions outside the range $0 \le R \le 1$, which are then clipped to that range.

Spline-Based Estimation

With this method (cubic spline), third order polynomials are adjusted between each pair of consecutive sampled points in such way that the resulting curve passes through the points and is continuous through the second derivative. The first and last polynomials can be used to extrapolate towards the blue and red ends of the spectrum. The simplest variation called natural cubic spline, which sets the second derivative to zero at the end points, cannot extrapolate the data well. Some rule is needed to keep the extrapolated spectra not too divergent from the sampled end points. In this study we chose to replicate at 400 and 700 nm the reflectances measured at the shortest and longest sampling wavelengths before fitting a natural cubic spline. This rule was retained after testing a few possibilities for the end point conditions and after observing that the simple replication for the end points made very little difference on color calculations compared to using the true reflectances at 400 and 700 nm. As with the PCA method, estimated reflectance values that fall outside the range 0..1 are clipped to that range.

Color Difference Calculation

The criterion that was employed for judging the goodness of a spectral estimation method with given wave-

lengths was to compare the average difference between true and estimated colors over some comprehensive data sets. The CIEDE2000 color-difference formula[14] was retained. With this formula, CIE tristimulus values X, Y and Z are first computed as the integral of the spectra weighted by the color matching functions of the standard colorimetric observer times the spectral power distribution of the CIE D65 standard illuminant. The X, Y and Z are next converted into CIE $L^*a^*b^*$ values.[15] The CIE DE2000 formula is designed to generate a number, ΔE_{00}, that correlates with the perceived difference between two colors of differing $L^*a^*b^*$ values. A ΔE_{00} of 1 roughly means that two colors are at threshold of visual differentiation when judged side-by-side under reference conditions. The CIEDE2000 formula is designed for color differences that are less than a few units. One issue is the choice among the 2º standard colorimetric observer and the 10º standard colorimetric observer for use in the calculations. Our understanding is that the standard viewing conditions that were used for the establishment of the CIEDE2000 formula call for the 10º standard colorimetric observer. On the other hand, colors measured with a digital imaging system are likely to vary within very small fields and one would think that the 2º standard colorimetric observer would be more appropriate. The 10º standard colorimetric observer was, however, retained throughout this study except for one test where the two observers were compared.

Wavelength Optimization

A function MeanError(λ_1, λ_2, …) is first implemented that returns the mean ΔE_{00} error over a collection for a given set of sampling wavelengths and for the particular estimation method considered:

MeanError(λ_1, λ_2, ...)
1. for each color sample of the set:
1.1. Read the reflectance $R(\lambda_1)$, $R(\lambda_2)$... from its true spectral reflectance curve $R_{true}(\lambda)$.
1.2. Estimate the spectral reflectance $R_{estimated}(\lambda)$ over the visible range.
1.3. Calculate CIE L^* a^* b^* values from the estimated spectrum as well as from the true spectrum.
1.4. Apply the CIEDE2000 color difference formula to the true and estimated $L^*a^*b^*$ to obtain ΔE_{00}.
2. Return the average ΔE_{00} over all the color samples.

The set of wavelengths that minimize the MeanError() function is then sought with the Nelder-Mead simplex method.[16] How the method works is best understood in the case of a search for three optimal wavelengths {λ_1, λ_2, λ_3}. The method then starts by building a small tetrahedron in three-dimensional space around some initial estimate. Vertices of the tetrahedron are then moved either away or closer to their opposing faces, or are projected through them, in order to make MeanError(λ_1, λ_2, λ_3) smaller. The tetrahedron eventually collapses around a minimum. The method generalizes to higher dimensionality of λ space, where the "hyper-tetrahedron" is called a simplex. The convergence of the method is still a topic of discussion among mathematicians.[17]

Data Sets

A first data set considered for the calculations refers to the 554 samples of the OSA-UCS color atlas. This color order system was designed in such way that the color difference between adjacent color points is perceptually constant. Each sample was measured in our laboratory with a Spectrogard II spectrophotometer for the 8°/diffuse geometry. The reflectance curves were re-sampled every 10 nm from 400 to 700 nm to produce column vectors of 31 components.

Five additional sets, identified here as COLORCHECKERDC, ESSER, GAMBLIN, NGAPANELS, and ROSS were obtained from Prof. R. S. Berns of the Rochester Institute of Technology. COLORCHECKERDC (240 samples with some neutrals replicated) and ESSER (283 samples) are commercial color charts used with digital cameras and scanners. GAMBLIN (63 samples) was fabricated using the Gambin conservation colors[18] which were mixed with white at two different concentrations. NGAPANELS (219 samples) is made of dry pigments dispersed in PVA, each pigment mixed with titanium white. These are the pigment collection of the National Gallery of Art, Washington (NGA). ROSS (68 samples) is artist oil paints, also mixed with titanium white, prepared by chief of conservation, Ross Merrill, at NGA.

TABLE I. Optimal Sets of Three, Four and Five Sampling Wavelengths for the PCA-Based Method Based on the Criterion of Minimum Mean CIEDE2000 Color Difference Over the Data Set. The CIE D65 Standard Illuminant and the CIE 10º Standard Observer Are Assumed.

Data set	Optimal wavelengths (nm)	Mean ΔE_{00}
OSA-UCS	443.4 534.0 608.5	1.7
COLORCHECKERDC	456.0 534.0 605.0	2.0
ESSER	447.5 535.5 601.1	2.1
NGAPANELS	441.9 536.0 613.8	2.4
GAMBLIN	443.8 535.2 600.9	2.8
ROSS	443.7 536.6 598.4	2.0
OSA-UCS	446.4 512.4 562.5 612.7	0.61
COLORCHECKERDC	445.9 517.6 564.6 614.7	0.75
ESSER	445.3 513.8 563.2 608.2	0.98
NGAPANELS	445.1 524.2 572.9 621.5	0.99
GAMBLIN	445.8 520.9 566.6 637.4	1.08
ROSS	446.8 512.6 554.7 608.5	0.75
OSA-UCS	442.0 496.1 536.7 581.6 618.1	0.34
COLORCHECKERDC	447.6 496.4 542.5 581.8 621.2	0.42
ESSER	443.0 493.4 530.7 572.5 613.3	0.48
NGAPANELS	446.1 496.9 536.3 581.6 623.0	0.65
GAMBLIN	445.2 487.6 531.8 574.5 617.3	0.63
ROSS	445.2 484.7 523.8 564.8 612.5	0.47

Optimal Wavelengths

Tables I and II give the sets of three, four, and five sampling wavelengths that were found to minimize the mean ΔE_{00} error for the six data sets using the PCA-based and the spline-based spectral estimation methods. As can be seen, the mean error is cut by about half going from three sampling wavelengths to four sampling wavelengths, and by another half going from four to five. The optimal wavelengths are fairly independent of the data set used to derive them, varying less than ±10 nm most of the time. Furthermore, this variability is higher when the number of wavelengths is larger, but the spectral estimation becomes less sensitive to the choice of wavelengths as their number increases.

The PCA-based method is seen to perform slightly better than the spline method. The advantage of the PCA-based method over the Spline method is at least true when the color to be estimated is part of the set that was used to derive the Principal Components and the optimal wavelengths. The sensitivity of the PCA method with respect to the "training set" used to derive the principal components was tested by performing a mean er-

TABLE II. Optimal Sets of Three, Four and Five Sampling Wavelengths for the Spline Method Based on the Criterion of Minimum Mean CIEDE2000 Color Difference Over the Data Set. The CIE D65 Standard Illuminant and the CIE 10° Standard Observer Are Assumed

Data set	Optimal wavelengths (nm)	Mean ΔE_{00}
OSA-UCS	456.3 533.4 607.3	2.1
COLORCHECKERDC	452.9 525.8 603.7	2.1
ESSER	453.3 536.3 596.8	2.4
NGAPANELS	443.8 536.6 605.4	2.3
GAMBLIN	444.7 537.2 602.0	2.8
ROSS	452.2 534.4 596.0	2.4
OSA-UCS	443.8 512.1 560.7 614.6	0.95
COLORCHECKERDC	444.3 514.0 564.0 615.0	0.98
ESSER	448.3 506.5 554.8 615.4	1.22
NGAPANELS	445.1 517.7 563.1 617.5	0.97
GAMBLIN	443.9 513.8 555.6 614.1	1.1
ROSS	446.5 507.0 555.1 613.8	1.1
OSA-UCS	443.8 511.9 557.5 597.8 633.7	0.55
COLORCHECKERDC	446.5 495.8 541.3 582.7 623.7	0.56
ESSER	443.6 494.4 532.5 573.5 617.4	0.67
NGAPANELS	444.1 514.1 556.2 596.3 641.2	0.67
GAMBLIN	443.7 511.8 550.9 592.2 640.8	0.75
ROSS	446.4 504.8 545.6 582.5 624.7	0.77

TABLE III. Mean ΔE_{00} Error, with the PCA-Based Method and Four Sampling Wavelengths, for Each Data Sets as a Function of the Training Set Used to Derive the Principal Components and the Optimal Wavelengths

	Data set used for training					
Data set	1	2	3	4	5	6
1:OSA-UCS	0.61	0.74	0.85	1.14	1.22	0.90
2: COLORCHECKERDC	1.02	0.75	1.03	1.44	1.38	1.04
3: ESSER	1.22	1.06	0.98	1.36	1.50	1.16
4: NGAPANELS	1.18	1.04	1.31	0.99	1.16	1.24
5: GAMBLIN	1.33	1.23	1.29	1.35	1.08	1.18
6: ROSS	1.01	0.97	1.02	1.13	1.22	0.75
Ave.:	1.15	1.01	1.13	1.26	1.27	1.07

TABLE IV. Predicted Mean CIE DE2000 Error Over the OSA-UCS Data Set for Some Combinations of Commercial Laser Wavelengths

Method	Set of laser wavelengths (nm)	Mean ΔE_{00}
Spline	442 532 633	3.0
PCA	442 532 633	3.1
Spline	442 532 568 633	1.3
Spline	442 514 568 633	1.4
PCA	442 514 568 633	1.5
PCA	442 488 532 568 633	0.88
Spline	442 488 532 568 633	0.94
Spline	442 514 532 568 633	1.1
Spline	442 488 514 532 568 633 647	0.92
PCA	442 488 514 532 568 633 647	0.93

ror calculation for each data set using the PCs and optimal wavelengths derived from each of the other five sets. Table III gives a matrix grid for these errors. The diagonal elements are smallest, as expected, and the off-diagonal elements are not too far away, which shows that the PCA-based method is not too sensitive to the training set used to derive the PCs and the optimal wavelengths. The COLORCHECKERDC appears to be the best training set among the six. This exercise was not repeated with the spline method because this method was found to be even less sensitive to variations of the sampling wavelengths than the PCA method.

The sensitivity of the optimal wavelengths to the choice of the Standard Colorimetric Observer was also tested by performing a few calculations with each of the observers inside the CIEDE2000 formula. The differences for the optimal wavelengths were found to be a few nanometers, at most, and were less than the variability relulting from the choice of data sets.

This is all indicative that optimal sets of three, four and five sampling wavelengths can be established, and that it is a bit vain to try to isolate these wavelengths to better than approximately ±5 nm. For example, the set {446 nm, 518 nm, 565 nm, 615 nm} and the method of calculation that uses the PCs and average reflectances from the Macbeth ColorCheckerDC, appears near-ideal when the goal is to keep the expected error to less than approximately one unit.

Near-Optimal Commercial Laser Lines

The NRC 3D camera requires TEM00 continuous wave lasers with power outputs roughly 10 mW or higher. It has been used in past years in a three lasers configuration, with HeCd (442 nm), DPSS green (532 nm) and HeNe (633 nm) simultaneously hooked to the camera through a single-mode optical fiber. We considered adding a ArKr tunable laser to the system, bringing a choice among 488 nm, 514 nm, 568 nm and 647 nm for additional wavelengths. Using Tables I and II as a guide, we tested various combinations of wavelengths that fell close to the optimal ones by predicting the mean error for the OSA-UCS catalog. Table IV presents these theoretical predictions.

As can be seen, the spline method and the PCA method become more-or-less equivalent for the sets of non-optimal wavelengths considered. There appears to be a substantial cost for deviating from the optimal wavelengths, specially with the PCA method. Most notable is the doubling of the predicted mean error when the non-optimal 633 nm red is used instead of the optimal 608 nm for scanning at three wavelengths. We believe the reason behind this is that many of the yellow-orange-red OAS-UCS samples owe their color to a rather sharp transition between low spectral reflectance values and high spectral reflectance values occurring somewhere in the $\lambda > 550$ nm region. Hue is very sensitive to the exact location of that transition. Spectral estimation methods can only approximate this transition with some sort of ramp between sampled green and sampled red. If the sampled red is too far towards the long wavelength limit on the axis, all the yellows, oranges and reds start looking orange-red since they are all approximated with the same ramp. The same idea applies to the blue-green shades but they seem less sensitive.

When fixed to using the HeNe 633 nm red, it appears very beneficial to incorporate a fourth sampling wavelength in the yellow region in order to catch the yellow-orange-red transition. The combination {442 nm, 532 nm, 568 nm, 633 nm} is seen to perform by a factor of two better than {442 nm, 532 nm, 633 nm} alone. There appears to be much less improvement to be gained from adding a fifth wavelength, either 488 nm or 514 nm, to catch the blue-green transition. Finally, introduction of

a sixth and a seventh wavelength does not bring significant improvement to the average color difference.

This exercise demonstrates the importance of being close to the optimal wavelengths, as the performance from scanning at all seven available wavelengths is still poorer than that predicted for four optimal wavelengths.

Experimentation

The next step was to get a practical sense of these predictions in the lab. It is possible to interface with the camera as many lasers as one wishes and capture the 3D-spectral images in multiple scans. Each laser line is then coupled to the camera through a single-mode optical fiber and used to capture a (3D + intensity) image of the object. Images captured with all the laser lines can then be merged into a single 3D multispectral image with the first three channels containing the (x,y,z) spatial information, and the rest of the channels containing the spectral reflectance at the sensing wavelengths. Ideally however, one would like to use just three or four lasers and benefit from the camera's optics and peak detection electronics that allow the simultaneous detection of up to four peaks. 3D multispectral acquisition in one single scan then becomes possible.

Many sources of uncertainty other than spectral estimation errors affect the color measurement results. These can be of systematic nature, e.g., calibration errors, dark signal offsets, etc., or purely random. An example of the latter is speckle noise that affects both the amplitude and centroid location of the peaks detected on the CCD.[19] Since these errors may dominate the spectral estimation errors, it is worth experimenting before investing in extra lasers and modified procedures.

For testing the performance of the color rendition system, a Macbeth Color Checker™ (we used the pocket size version of this chart) and a Macbeth Color Checker DC™ were scanned at all seven wavelengths available to us. A first scan was with the HeCd, DPSS green and HeNe lasers coupled simultaneously to the camera. This was followed by four additional scans with the extra wavelengths from the ArKr laser coupled one line at a time. CRT renderings of the charts were then produced for various combinations of the wavelengths, allowing visual judgment.

The following steps are involved in the experimental workflow:

1. An intensity calibration model is first established prior to scanning the objects. This is extracted from series of scans of a nearly-Lambertian white reference target placed at various depths inside the volume. The spatial dependence of the intensity response of the camera over its whole 3D volume of view is then determined. This is repeated for each scanning wavelength.
2. After a given object is scanned, the calibration model is used to recover reflectance values at each surface element (surfel). A compensation for shading effects, which makes use of the 3D information and exploits a BRDF model,[11] is embedded in this step as well as in step 1.
3. For each surface element, an associated full visible spectrum is estimated based on the reflectance values for the chosen set of sampling wavelengths. The spline interpolation method was favored for this test.
4. CIE XYZ tristimulus values for the D65 standard illuminant and the 2° standard observer are then derived from the estimated spectrum.
5. CIE XYZ tristimulus are next converted into sRGB values.[20] (Note that the 2° observer is imposed by the sRGB standard while CIEDE2000 applies to the 10° observer; this is nevertheless consistent since there is no relationship between the standard used for encoding and the standard used for color difference evaluation.)
6. The sRGB part of the 3D color image is finally displayed on a CRT operated close to the sRGB standard conditions.

We note that our testing made use of flat 2D charts placed nearly perpendicular to the camera's and viewer's lines of sight. The 3D information served only at the reflectance recovery stage. For more complicated 3D shapes, synthetic shadows would be applied on the virtual objects for realistic renderings. This shadowing must be performed in *XYZ* color space prior to conversion to sRGB.

For the comparison, the CRT was placed next to a Macbeth viewing booth simulating daylight and holding the real charts. The visual comparison confirms that the combination {442 nm, 532 nm, 633 nm} fails to deliver the pure reds, which are rendered orange-red instead. Other "warm" colors suffer as well. This problem appears to be solved with the addition of the 568 nm wavelength. The large majority of the colors of the charts then reproduce well, at least as far as can be judged with this kind of test. Although some visible improvement could be observed with the addition of a fifth wavelengths at 488 nm, this improvement was found to be very subtle and probably not worth the extra cost.

In order to provide a more quantitative judgment of the goodness of the experimental results, we measured the 24 samples of our small Macbeth ColorChecker with a NRC-traceable Perkin Elmer Lambda 19 (PE-19) spectrophotometer, for the 0/45 geometry. The PE-19 reflectance data, resampled every 10 nm from 400 to 700 nm, served as a reference to calculate the "true" CIELAB values and the "predicted" spline estimated CIELAB values that should result from sampling with the four laser combination {442 nm, 532 nm, 568 nm, 633 nm}. The "experimental" laser scanner CIELAB values, for these particular four wavelengths, were extracted from the sRGB image generated with the system. The mean and the standard deviation of the experimental CIELAB values were computed for regions of interest (ROI) comprising a few thousands of pixels. The standard deviation of each of the $L^*a^*b^*$ components, inside a given ROI, is typically of the order of 2 CIELAB units and corresponds to the magnitude of the random noise affecting the system. The means are taken as the "experimental" CIELAB values. Figure 1 shows in a^*b^* space the distribution of the true, predicted and experimental values. The difference between the experimental CIELAB values and the predicted CIELAB values corresponds to the systematic errors of instrumental origin. The difference between the predicted and the true CIELAB values corresponds to the systematic error inherent to the spectral estimation method by itself. These two types of error appear to be of similar magnitude. We note that the a^*b^* differences tend to be higher for the highly chromatic colors, but that this is partially compensated by the CIEDE2000 formula which scales down a^*b^* differences with increasing chroma.

Conclusion

3D autosynchronized laser scanning at a number of discrete wavelengths is a powerful technique for capturing surface reflectance values from objects, in perfect registration with the spatial coordinates of the surface

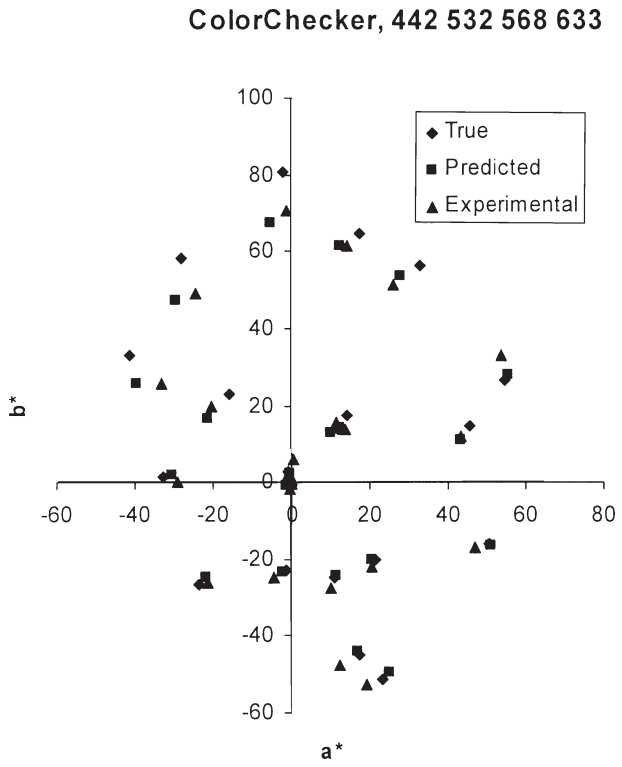

Figure 1. Comparison, for the Macbeth ColorChecker, of the experimental a*b* values with the true and the predicted values derived from measurements with a NRC-traceable Perkin Elmer Lambda-19 spectrophotometer. The experimental data are for the laser scanner operated with four laser wavelengths 442 nm 532 nm, 568 nm and 633 nm, and using the spline-based spectral estimation method for color calculations.

elements and without inter-reflection problems. When the reflectance data is used to calculate the perceptual color values of the surface elements, the choice of the laser lines used for scanning affects the achieved color accuracy. In virtual reality applications, there is no need to be more accurate than what the graphics engine can deliver and what the visual system can detect. In consequence one can limit the number of wavelengths to something practical.

We started this study by deriving optimal sets of three, four and five sampling wavelengths through simulations that made use of available color reflectance data sets and of the recently proposed CIEDE2000 color difference formula. These wavelengths were identified to within approximately ±5 nm. A combination of four wavelengths appears sufficient to bring the expected colorimetric error to less than approximately 1 CIEDE2000 unit.

In light of the above findings, we next investigated the best combination of practical laser lines available on the market. For this we predicted the mean ΔE_{00} error over the OSA-UCS collection for various combinations of HeCd, ArKr, HeNe and DPSS laser lines. The best combinations of three, four and five wavelengths were found to be {442 nm, 532 nm, 633 nm}, {442 nm, 532 nm, 568 nm, 633 nm} and {442 nm, 488 nm, 532 nm, 568 nm, 633 nm}. Performance is predicted to degrade substantially using these commercial lines instead of the unconstrained optimal ones. Sensing in the green-yellow to orange-red region of the spectrum was found critical for proper rendition of the pure reds.

Our theoretical predictions were finally tested in the lab by coupling the camera to seven different lasers lines and capturing 3D-multispectral images of color charts. For the laser lines we tested, a four wavelengths combination appeared necessary for the capture of the red shades. Incorporation of additional wavelengths was found to bring only marginal improvement. This holds true for the color charts that were used, which are believed to be representative of a large fraction of the color surfaces encountered in real life. Finally, we find that the laser scanner systematic errors, which are due to influential factors other than the spectral estimation method itself, appear comparable to the spectral estimation errors.

Acknowledgment. The author wish to thank Professor Roy S. Berns for contributing his reflectance data sets, Dr. Zoltan Jakab for his work in our lab on the measurement of the OSA-UCS samples, and Luc Cournoyer for the technical realization of the multispectral laser scans.

References

1. CIE 15.*2 Colorimetry,* 2nd ed., CIE Publ. 15.2. CIE Central Bureau, Vienna, 1986.
2. R. S. Berns and F. H. Imai, The use of multi-channel visible spectrum imaging for pigment identification, *Proc. ICOM Committee for Conservation, 13th Triennial Meeting,* 2002, p. 217.
3. H. Liang, D. Saunders, J. Cupitt, and M. Benchouika, A new multispectral imaging system for examining paintings, *Proc. CGIV 2004: The Second European Conference on Colour Graphics, Imaging and Vision*, IS&T, Springfield, VA, 2004, p. 229.
4. C. Balas, V. Papadakis, N. Papadakis, A. Papadakis, E. Vazgiouraki, and G. Themelis, A novel hyper-spectral imaging apparatus for the non-destructive analysis of objects of artistic and historic value, *J. Cultural Heritage* **4,** 330 (2003).
5. C. Lahanier, G. Alquié, P. Cotte, C. Christofides, C. de Deyne, R. Pilay, D. Saunders, and F. Schmitt, Color and multispectral imaging with the CRISATEL multispectral system, *Proc. IS&Ts PICS Conf.,* IS&T, Springfield, VA, 2003, p. 215.
6. R. Baribeau, L. Cournoyer, G. Godin, and M. Rioux, Colour Three-Dimensional Modeling of Museum Objects, *Imaging the Past*, British Museum Occasional Paper no. 114, T. Higgins et al., Eds., The British Museum, London, UK, 1996, pp. 199-209.
7. J. Taylor, J. A. Beraldin, G. Godin, L. Cournoyer, R. Baribeau, F. Blais, M. Rioux, and J. Domey. NRC 3D imaging technology for museum and heritage applications, *J. Visual. Comput. Animat.* **14,** 121 (2003).
8. G. Godin, J.-A. Beraldin, J. Taylor, L. Cournoyer, M. Rioux, S. El-Hakim, R. Baribeau, F. Blais, P. Boulanger, M. Picard, and J. Domey, Active optical 3-D imaging for heritage applications, *Proc. IEEE Comp. Graph. Appl.* **22,** 24 (2002).
9. M. Soucy, G. Godin, R. Baribeau, F. Blais, and M. Rioux. Sensors and algorithms for the construction of digital 3-D colour models of real objects, in *Proc. IEEE International Conference on Image Processing (ICIP-96)* Vol. II, IEEE Press, Los Alamitos, CA, 1996, p. 16.
10. M. Rioux, Laser range finder based on synchronized scanners, *Appl. Opt.* **23,** 3837 (1984).
11. R. Baribeau, M. Rioux and G. Godin, Color Reflectance Modelling Using a Polychromatic Laser Range Sensor, *IEEE Trans. Pattern Anal. Machine Int.* **14,** 263 (1992).
12. B. K. P. Horn, Exact reproduction of colored images. *Comp. Vision, Graph. Image Process.* **26,** 135 (1984).
13. H. S. Fairman and M. H. Brill, The principal components of reflectances, *Color Res. Appl.* **29,** 104 (2004).
14. *Improvement to Industrial Colour-Difference Evaluation*, CIE Publ. 142, CIE Central Bureau, Vienna, 2001.
15. *Industrial Colour-Difference Evaluation*, CIE Publ. 116, CIE Central Bureau, Vienna, 1995.
16. J. A. Nelder and R. Mead. *Computer J.* **7,** 308 (1965).
17. J. C. Lagarias, J. A. Reeds, M. H. Wright, and P. E. Wright, Convergence properties of the Nelder-Mead simplex method in low dimensions, *SIAM J. Optim.* **9,** 112 (1998).
18. http://www.gamblincolors.com/conservation/products/colors.html.
19. R. Baribeau and M. Rioux. Influence of speckle on laser range finders. *Appl. Opt.* **30,** 2873 (1991).
20. *Colour Measurement and Management in Multimedia Systems and Equipment, Part 2-1: Colour Management -Default RGB Colour Space-sRGB*, IEC 61966-2-1, International Electrotechnical Commission, Geneva, Switzerland, 1999.